Figures and figure supplements

SARS-CoV-2 requires cholesterol for viral entry and pathological syncytia formation

David W Sanders *et al*

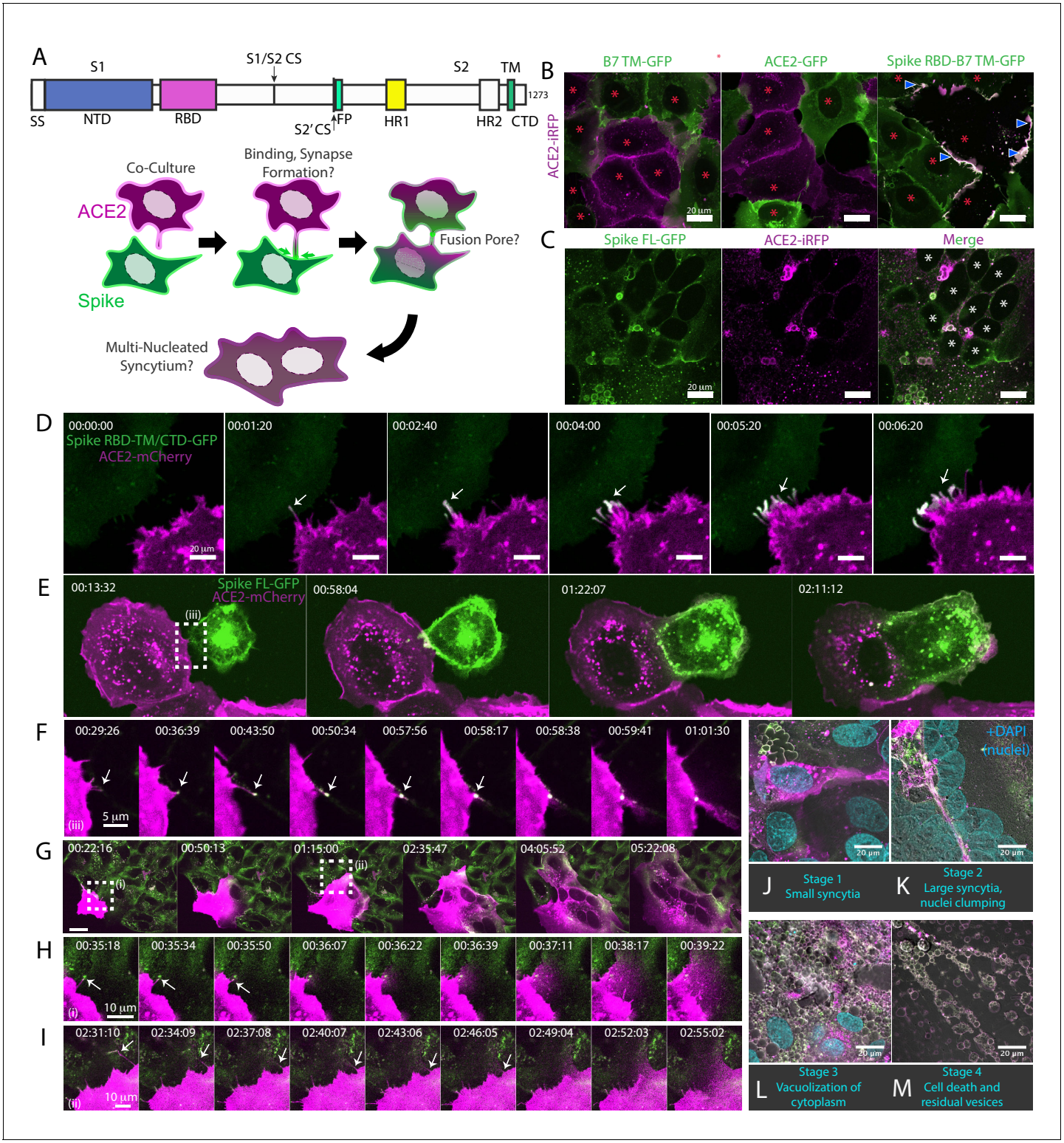

Figure 1. Syncytia derive from fusion events at synapse-like, spike-ACE2 protein clusters. (**A**) Top: Domain structure of a single monomer of the SARS-CoV-2 spike trimer. Domains/motifs is from left to right (see KEY RESOURCES table for residue boundaries): SS (signal sequence), NTD (N-terminal domain), RBD (receptor-binding domain), S1/S2 (subdomain-1/2 cleavage site), S2′ (subdomain-2′ cleavage site), FP (fusion peptide), HR1 (heptad repeat 1), HR2 (heptad repeat 2), TM (transmembrane alpha helix), CTD (cytoplasmic domain). Bottom: Cartoon depiction of live cell co-culture assays to detect spike-ACE2 binding and cell-cell fusion. Magenta, acceptor cells (human ACE2-mCherry or ACE2-iRFP); Green, donor cells (GFP-tagged spike variant). (**B**) ACE2-iRFP U2OS (human osteosarcoma) acceptor cells (magenta) co-cultured for 24 hr with U2OS cells expressing GFP-tagged proteins

Figure 1 continued on next page

Figure 1 continued

(green): B7 transmembrane (TM, left), ACE2 (middle), spike receptor-binding domain (RBD-TM/CTD, right). Red asterisks indicate single cell nuclei in isolation (no syncytia); arrowhead, synapses (select examples noted). (**C**) Co-culture of U2OS acceptor cells expressing ACE2-iRFP (magenta) with spike full-length ('FL')-GFP U2OS cells (green). White asterisks: cell nuclei in syncytium. (**D**) Co-culture of ACE2-mCherry (magenta) and spike RBD-TM/CTD-GFP (green) cells for indicated amount of time (hours:minutes:seconds). Arrow: synapse-like interfaces between cells. Scale-bar, 5 μm. See also ***Figure 1—video 1*** for long-lived ACE2-Spike FL synapses. (**E**) Similar to (**D**), but spike FL-GFP and ACE2-mCherry co-culture. Dashed box indicates site of synapse formation and cell-cell fusion. See ***Figure 1—video 2*** for time-lapse movie. (**F**) Zoom-in on synapse formation (arrow, left image) and fusion event (arrow, sixth image from left) of dashed box in (**E**). (**G**) ACE2-mCherry cell added to pre-plated spike FL-GFP U2OS cell monolayer (time since ACE2 cell plating indicated). Syncytium forms by multiple cell-cell fusion events (dashed boxes). See (**H,I**) for zoom-in events (i) and (ii). See ***Figure 1—video 3*** for time-lapse movie. (**H**) First cell fusion event (i from **G**) at spike-ACE2 synapse. Time since ACE2-mCherry cell plating indicated. Arrow: retracting synapse prior to cell fusion. (**I**) Similar to (**H**) but second cell-cell fusion event (ii from **G**). (**J**) Representative image of small syncytia (stage 1) common at early time points following co-culture of ACE2-mCherry (magenta) and spike-GFP (green) U2OS cells but rare at 24 hr (blue, Hoechst DNA stain). (**K**) Similar to (**J**), but representative of more common, larger syncytia (stage 2) at 24 hr. Nuclei (blue) clump in center of syncytium. (**L**) Similar to (**J**), but representative of typical syncytium with extensive vacuolization (stage 3) at 48 hr. (**M**) Similar to (**J**), but representative of remnants (spherical membranous structures) of dead syncytium at 72 hr (stage 4). See also ***Figure 1—figure supplement 1***; ***Figure 1—video 1–3***.

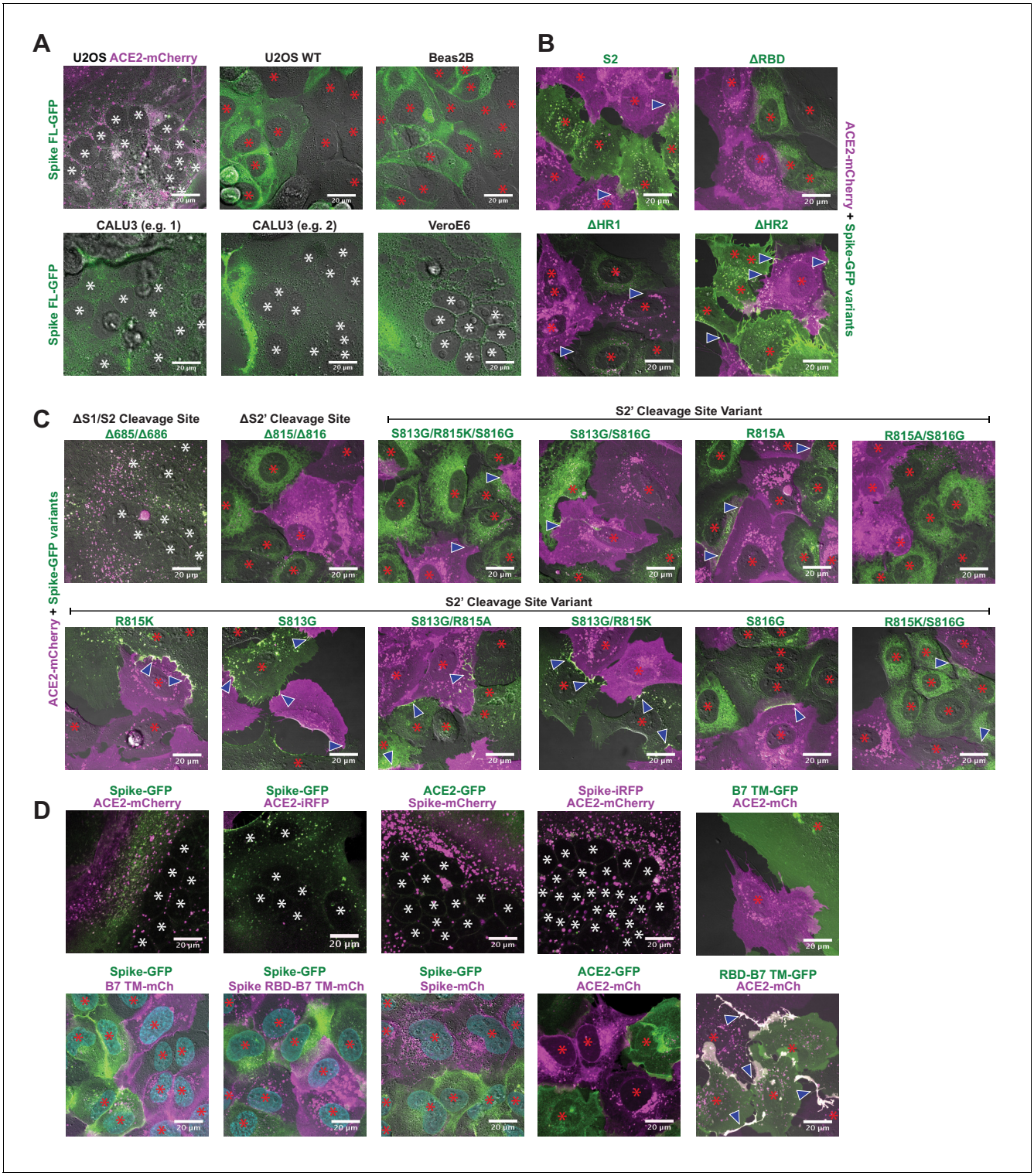

Figure 1—figure supplement 1. Syncytia derive from fusion events at synapse-like, spike-ACE2 protein clusters. (**A**) Indicated non-transduced cells (or ACE2-mCherry/U2OS control) co-cultured with U2OS spike-GFP (green) cells for 24 hr. White asterisks indicate nuclei in syncytia; red, in isolation. (**B**) Indicated GFP-spike variant (green) U2OS cells co-cultured with U2OS ACE2-mCherry (magenta) cells for 24 hr. White asterisks indicate nuclei in syncytia; red, in isolation; arrowhead, synapses (select examples noted). (**C**) Similar to (**B**), but using spike variants that disrupt its two cleavage sites (S1/S2 vs. S2'). (**D**) U2OS cells expressing spike or ACE2 with indicated fluorescent tag, co-cultured for 24 hr. White asterisks indicate nuclei in syncytia; red, in isolation; arrowhead, synapses (select examples noted).

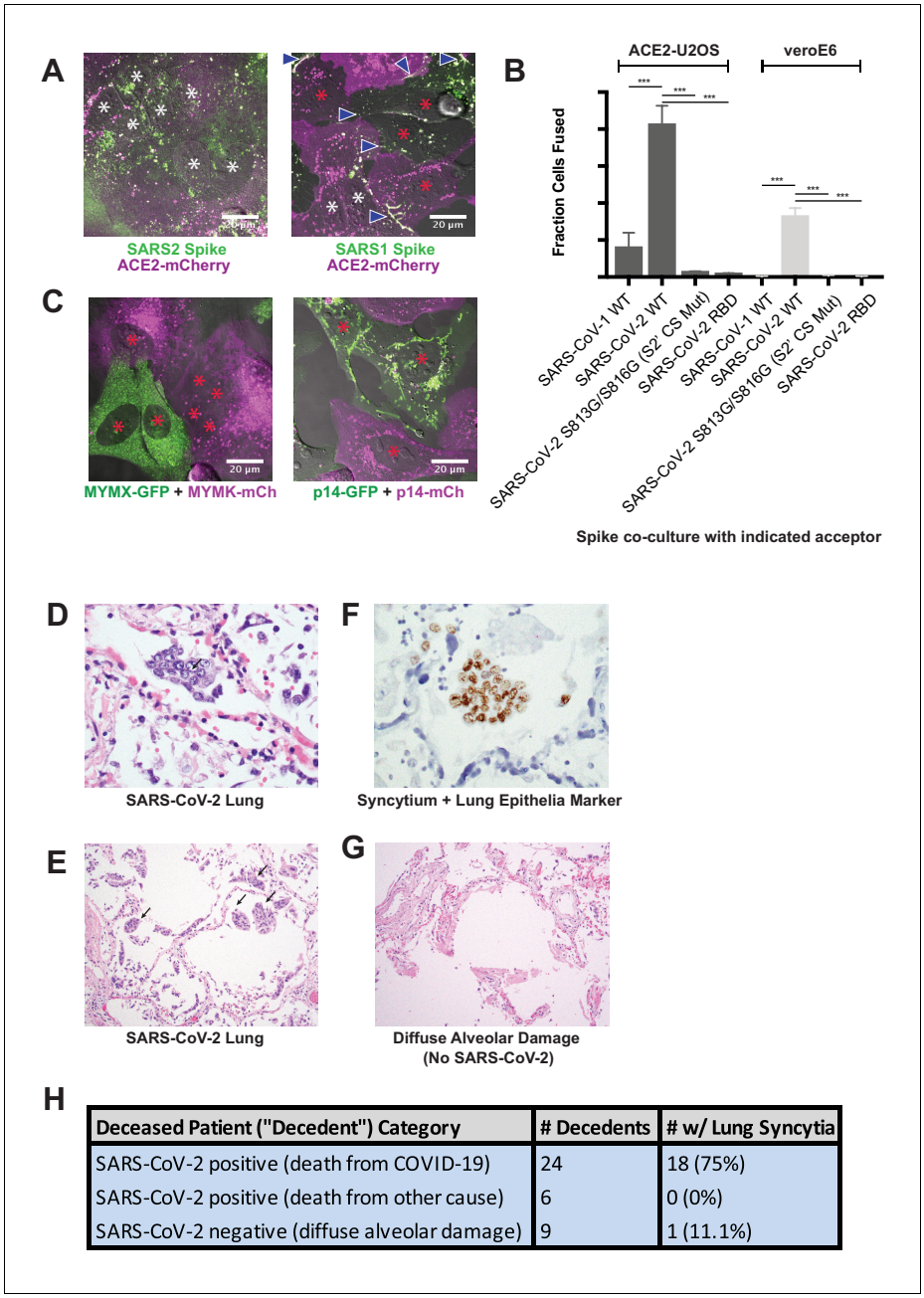

Deceased Patient ("Decedent") Category	# Decedents	# w/ Lung Syncytia
SARS-CoV-2 positive (death from COVID-19)	24	18 (75%)
SARS-CoV-2 positive (death from other cause)	6	0 (0%)
SARS-CoV-2 negative (diffuse alveolar damage)	9	1 (11.1%)

Figure 2. Syncytia are a defining pathological feature of COVID-19. (**A**) ACE2-mCherry (magenta) U2OS cells co-cultured with GFP-tagged (green) SARS-CoV-2 spike cells (left) or SARS-CoV-1 spike cells (right) for 24 hr. White asterisks indicate nuclei in syncytia; red, in isolation; arrowhead, synapses (select examples noted). (**B**) Quantification of (**A**) by percent cells fused (also tested VeroE6 donor cells, which express endogenous ACE2, and control SARS-CoV-2 spike variants that lack ability to promote fusion). Mean and SEM: n = 4 biological replicates (16 images per). p-Values of <0.01, <0.001, and<0.0001 are represented by *, **, and ***, respectively. (**C**) Indicated fusogen-expressing cells lines co-cultured for 24 hr. Red asterisk indicates nuclei of single cells (not in syncytia). (**D**) Lung from SARS-CoV-2 decedent demonstrating syncytia formation (H and E stained section, ×400 original magnification). Syncytium labeled with arrow. (**E**) Similar to (**D**), but sample obtained from different deceased COVID-19 patient and at ×100 magnification. Syncytium labeled with arrow. (**F**) Immunohistochemistry for lung epithelia marker TTF-1 (NKX2-1; brown) showing nuclear positivity in the syncytial cells (×400 original magnification). (**G**) Lung from control decedent with diffuse alveolar damage unrelated to SARS-CoV-2 infection (died pre-2019), showing hyaline membranes (remnants of dead cells; bright pink) but no syncytia (H and E stained section, ×100 original magnification). (**H**) Table summarizing decedents examined for syncytia pathology.

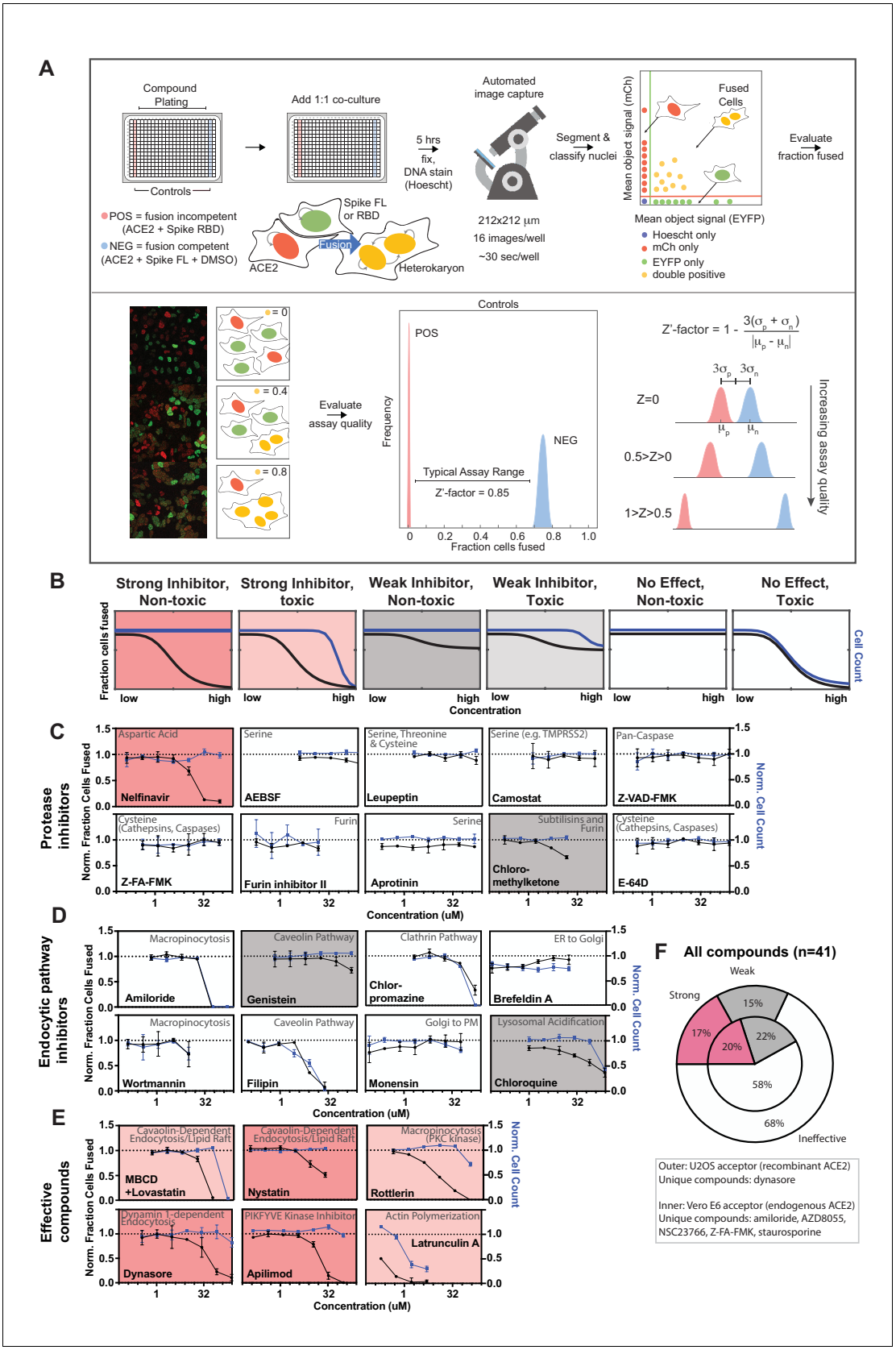

Figure 3. A novel high-throughput screening platform identifies modulators of syncytia formation. (**A**) Heterokaryon assay workflow overview (top) and characterization (bottom). Equal parts acceptor cells (express ACE2-iRFP and FUS-mCherry) plus donor cells (express spike FL-iRFP and HNRNPA1-

Figure 3 continued on next page

Figure 3 continued

EYFP) are co-cultured in 384-well microtiter plate: positive control (spike RBD, red column), negative control (DMSO, blue column), test compounds (other columns). After 5 hr, cells are fixed and nuclei are stained (Hoechst) then identified/segmented by automated confocal microscopy. Fraction cells fused is determined by percent co-positive (mCherry and EYFP) nuclei. Sample images and schematic interpretation of a positive control well (top), test well with reduced fusion (middle), negative control well (bottom). Z'-factor measures window size with higher score indicating a more robust screening platform. (**B**) Schematic of assay dose-response and interpretation. Fraction of cells fused (black curve) relative to cell count (toxicity measure, blue curve), both normalized by plate negative control, indicate compound efficacy (pink, strong inhibitor; gray, weak inhibitor; white, no-effect). Compounds are designated as effective if the maximum dose z-score is <-3. Strong vs. weak inhibitor designation is based on an arbitrary cutoff. (**C**) A panel of spike protease inhibitors (n = 10), which includes antagonists of both established SARS-CoV-2 entry pathways (cathepsin-dependent endocytosis vs. TMPRSS2/furin-mediated direct fusion), was tested. Mean and SEM: n = 4 biological replicates (16 images per). (**D**) Similar to (**C**), but displaying dose-response relationships for select inhibitors of indicated routes of endocytosis (e.g. clathrin, macropinocytosis) and steps in secretory pathway (e.g. ER-Golgi transport). See ***Figure 3—figure supplement 1F*** for additional tested compounds. (**E**) Similar to (**C**), but displaying dose-response relationships for compounds that strongly inhibit cell-cell fusion in ACE2-U2OS heterokaryon assay. See ***Figure 3—figure supplement 2*** for similar effect in VeroE6 assay (no exogenous ACE2 expression). (**F**) Summary of targeted drugs (n = 41) in U2OS and Vero based co-culture assays. Identified inhibitors are largely similar between cell types. Cell type-specific effects are noted. See also ***Figure 3—figure supplements 1–2***; ***Supplementary file 4***.

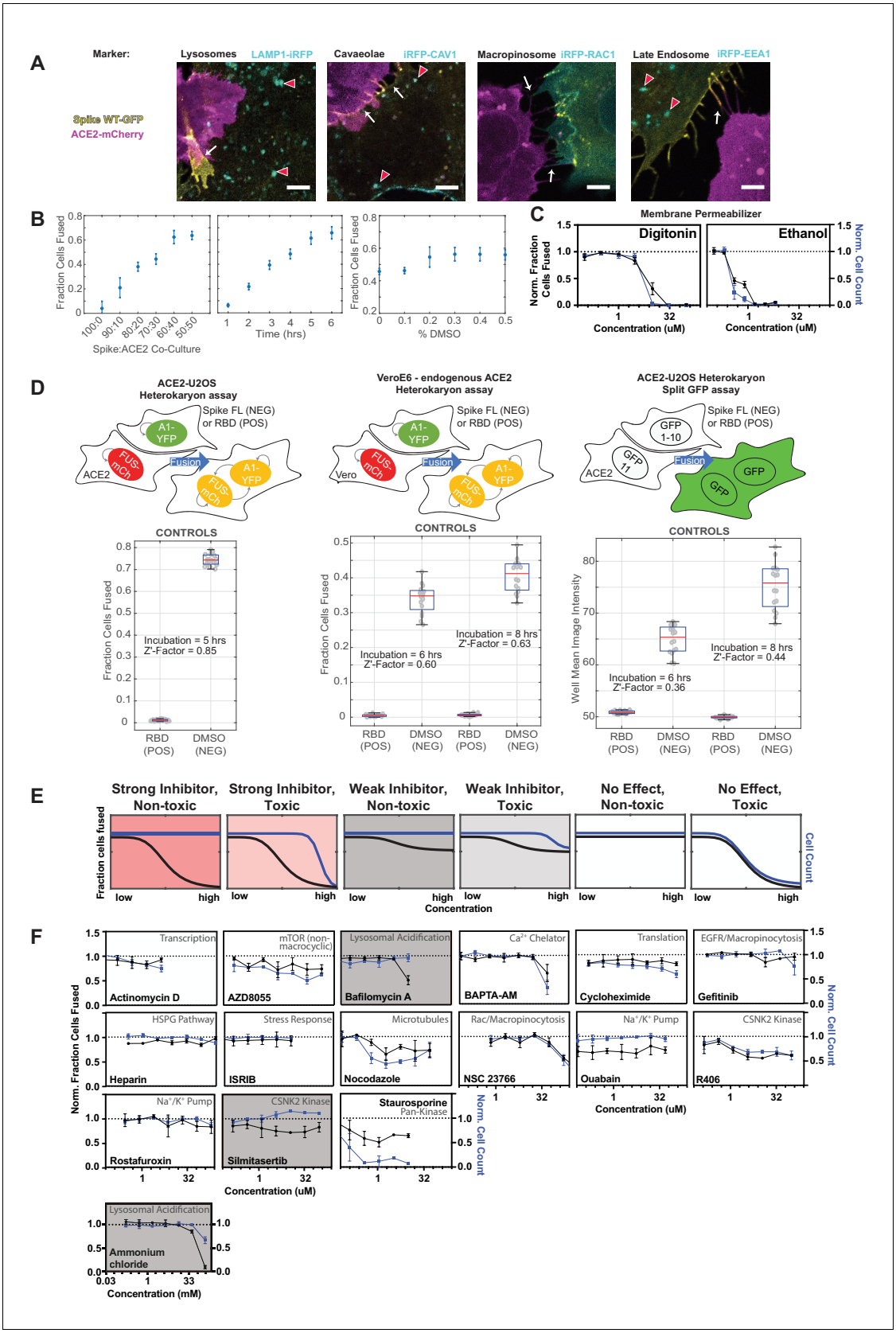

Figure 3—figure supplement 1. A novel high-throughput screening platform identifies modulators of syncytia formation. (**A**) U2OS cells co-expressing spike-GFP (yellow) and iRFP-tagged (cyan) endocytic markers (indicated) co-cultured with ACE2-mCherry (magenta) cells, with cell-cell fusion events

Figure 3—figure supplement 1 continued on next page

Figure 3—figure supplement 1 continued

assessed by live cell microscopy. Representative images show lack of co-localization between spike and iRFP-tagged proteins at synapses (white arrows) and vesicles (red arrowheads) prior to fusion. Scale-bar, 5 μm. (**B**) Optimization of ACE2-U2OS heterokaryon assay. Co-cultures were performed and fusion was quantified upon altering: spike to ACE2 cell ratio (left); length of co-culture time prior to fixation (middle); DMSO concentration (right). Default experimental parameters: 1-to-1 ratio, 5 hr, 0.5% DMSO. Mean and SEM: n = 4 biological replicates (16 images per). (**C**) Dose-response for membrane-permeabilizing compounds in ACE2-U2OS heterokaryon assay. Cell count (blue) and fraction fused (black) curves are similar, indicating lack of toxicity-independent inhibition of cell-cell fusion. Mean and SEM: n = 4 biological replicates (16 images per). (**D**) Comparison of three different heterokaryon microscopy assays, each of which use fluorescent proteins as readouts for fusion. Bottom: relative fusion for positive (spike RBD donor cells; fusion-incompetent) and negative (spike full-length donor cells + DMSO; fusion-competent) controls for indicated assay (top, with graphical depiction) with measured Z'-factor, which indicates assay strength (higher = more robust). Mean and SEM: n = 4 biological replicates (16 images per). (**E**) Schematic of ACE2-U2OS assay dose-response and interpretation. Fraction of cells fused (black curve) relative to cell count (toxicity measure; blue curve), both normalized by plate negative control, indicates compound efficacy (pink, strong inhibitor; gray, weak inhibitor; white, no-effect). (**F**) Dose-response relationships for additional compounds tested in ACE2-U2OS heterokaryon assay. Mean and SEM: n = 4 biological replicates (16 images per). See ***Figure 3—figure supplement 2*** for same compounds in VeroE6 heterokaryon assay.

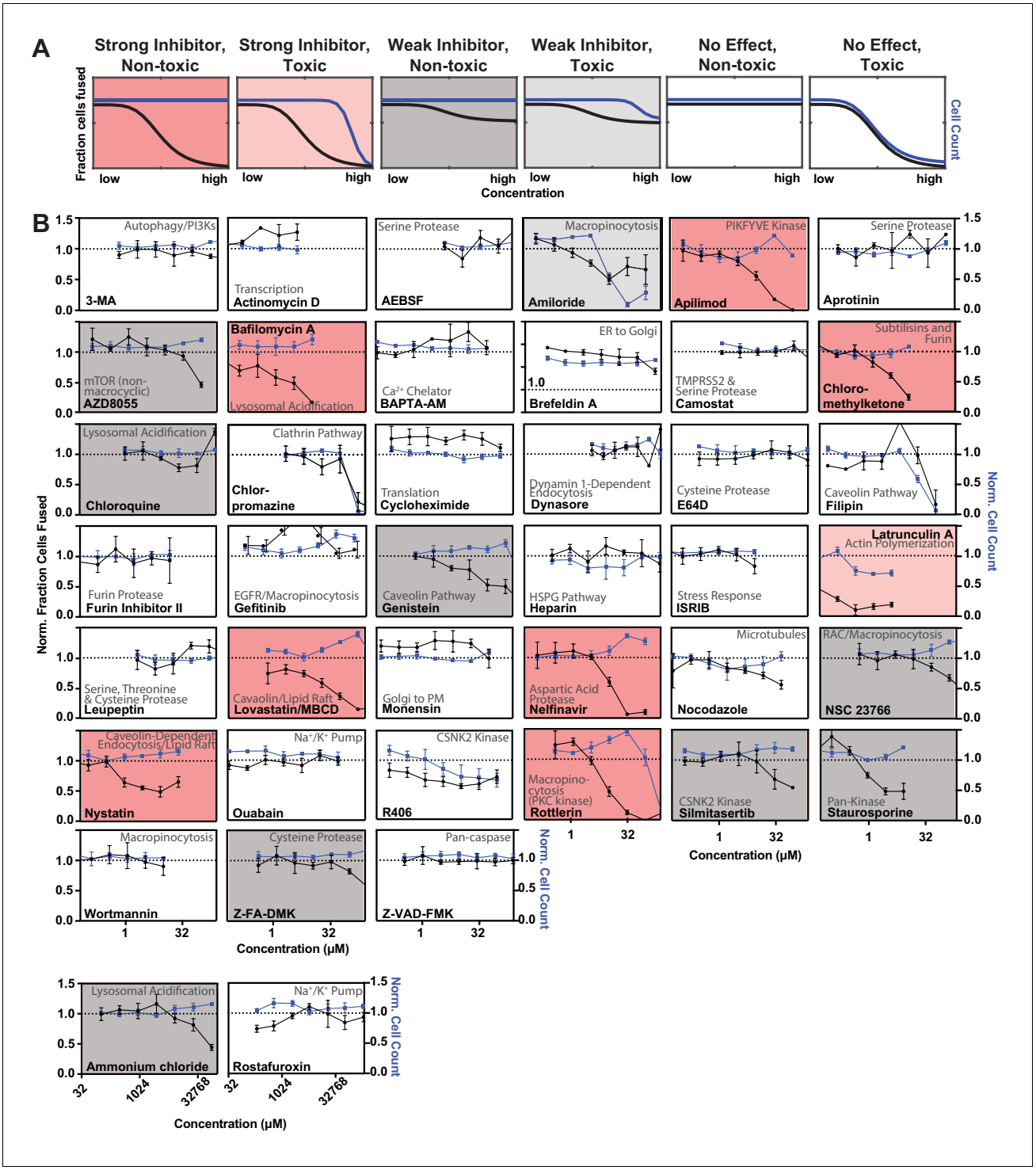

Figure 3—figure supplement 2. A novel high-throughput screening platform identifies modulators of syncytia formation. (**A**) Schematic of VeroE6 heterokaryon assay (no exogenous ACE2 overexpression) dose-response and interpretation. Fraction of cells fused (black curve) relative to cell count (toxicity measure; blue curve), both normalized by plate negative control, indicates compound efficacy (pink, strong inhibitor; gray, weak inhibitor; white, no-effect). (**B**) Dose-response relationships for all compounds (n = 41) tested in VeroE6 heterokaryon assay. Mean and SEM: n = 4 biological replicates (16 images per). See ***Figure 3*** and ***Figure 3—figure supplement 1*** for effect of same compounds in ACE2-U2OS heterokaryon assay.

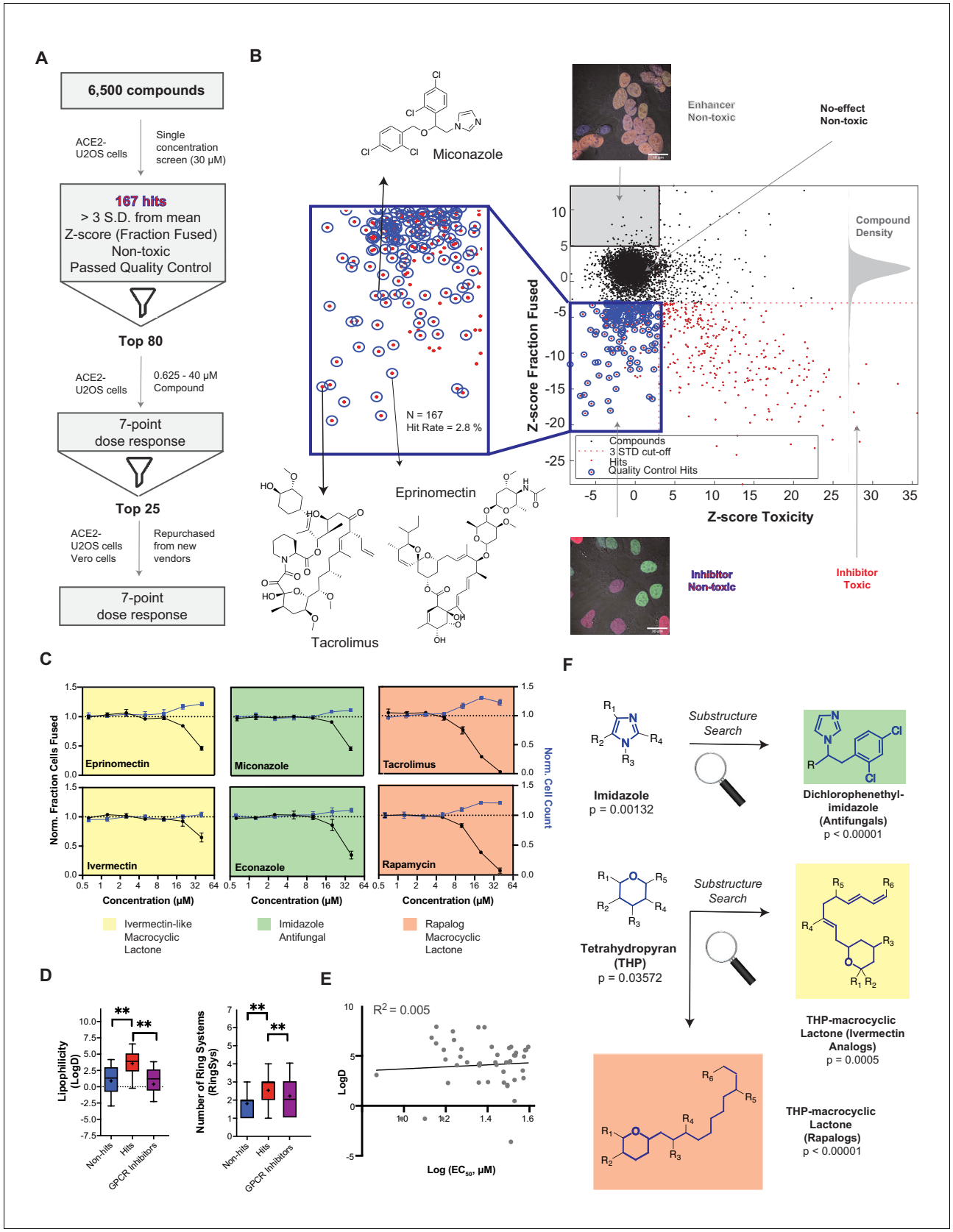

Figure 4. A drug repurposing screen implicates membrane lipid composition in cell-cell fusion. (**A**) High-throughput pipeline and workflow of small molecule screen (~6000 compounds, 30 µM) in ACE2-U2OS heterokaryon assay. 'Hits' refer to non-toxic compounds with a decrease in fusion of >3

Figure 4 continued on next page

Figure 4 continued

standard deviations relative to plate negative control. 7-point dose-response was determined for top-80 inhibitors, followed by validation of select compounds (n = 24; obtained from different vendors) in both ACE2-U2OS and VeroE6 heterokaryon assays. (**B**) Results of compound screen. Plot: fraction fused vs. toxicity z-score. Red dots indicate compounds with decreased fusion (z-score<-3); blue inset, potential hits following toxicity filtering (z-score <3); blue circles, quality-controlled hits (inhibitory, non-toxic compounds with normal fluorescence); gray inset, compounds with increase in fraction cells fused (z-score >5) but no toxicity ('enhancers', see ***Figure 6J***); right histogram, compound density as function of fraction fused z-score. Chemical structures are displayed for select validated hits. See ***Supplementary file 1*** for raw data. (**C**) Dose-responses for select hits in enriched substructure classes (see **F**): imidazoles (e.g. azole antifungals, green) and macrocyclic lactones (ivermectin-like, yellow; rapalogs, pink). Mean and SEM: n = 3 biological replicates (16 images per). (**D**) Box-and-whisker plots of select physicochemical properties (lipophilicity, logD; ring systems) for non-hits (blue), inhibitory hits (red), and GPCR inhibitors (purple) as calculated in ChemAxon. Boxes encompass 25–75% of variance; whiskers, 10–90%. Mean values are indicated by '+"; median values, lines. Statistical significance was assessed by Mann-Whitney U test: p-values of <0.05 and<0.001 are represented by * and **, respectively. (**E**) Lack of correlation between inhibitory hit EC_{50} (see ***Figure 4—figure supplement 1A***) and lipophilicity according to linear regression analysis conducted in GraphPad Prism. (**F**) Three substructure classes based on two scaffolds were identified to have high statistical enrichment in hits over non-hits: dicholorophenethyl-imidazoles (found in azole antifungals, green) and tetrahydropyrans with alkyl moieties (found in macrocyclic lactones; yellow and pink indicate ivemectin-like and rapalog compounds, respectively). See also ***Figure 4—figure supplements 1–2***; ***Supplementary file 1***.

A

	U2OS		*	U2OS		Vero			U2OS		*	U2OS		Vero	
Compound	EC50	N[1]	*	EC50	N	EC50	N	Compound	EC50	N	*	EC50	N	EC50	N
PD-407824	7.40	0.79	*	40.00	1.05	11.40	1.10	Vorapaxar	33.65	1.18	*	40.00	1.10	8.70	1.09
Chlorhexidine acetate	9.75	1.13	*	10.45	1.06	2.53	1.02	Isavuconazonium sulfate	33.79	1.08					
Chlorhexidine hydrochloride	12.59	1.06						Apomorphine hydrochloride	33.80	1.11	*	40.00	1.03	40.00	1.07
Pimecrolimus	13.57	1.23						Vorapaxar sulfate	34.11	1.17					
UK-356618	14.26	1.10	*	18.80	1.05	8.26	1.05	Econazole nitrate	34.33	1.11					
TW-37	14.30	1.15	*	11.23	1.10	4.86	1.01	Canagliflozin	37.02	1.11	*	40.00	1.13	17.91	1.12
Chlorohexidine dihydrochloride	15.25	1.02						Avanafil	37.29	1.14	*	40.00	1.02	28.40	1.02
Tacrolimus	15.50	1.28						Thonzonium bromide	37.53	0.75					
Isopomiferin	15.80	1.01						Eprinomectin	37.97	1.22					
JFD00244	15.92	1.11	*	32.69	1.10	7.92	1.10	Ritanserin	38.06	0.86	*	40.00	1.10	19.28	1.07
Ticagrelor	16.24	1.09	*	16.75	1.16	7.67	1.07	Tacrolimus	38.42	1.19					
Rapamycin	17.14	1.23	*	17.33	1.20	8.90	1.08	Miconazole nitrate	39.30	1.08					
BML-266	17.36	1.18						(±)-Epinephrine hydrochloride	40.00	0.96					
Rolapitant hydrochloride	17.93	1.19	*	17.90	1.14	9.56	1.02	6,7-ADTN hydrobromide	40.00	1.05					
TAK-285	18.61	1.01	*	15.88	1.16	6.87	1.11	BIRB 796 (Doramapimod)	40.00	1.07					
Moxidectin	18.85	1.12	*	25.09	0.95	6.20	1.04	BYL719	40.00	0.79					
AMG 9810	19.60	1.24	*	22.43	1.11	3.79	1.05	CAY10581	40.00	0.94					
Aprepitant	20.05	1.18						Chloro-IB-MECA	40.00	1.13					
Gossypol	22.69	1.11	*	20.43	1.06	17.00	1.07	Clofarabine	40.00	1.07					
Indacaterol maleate	22.79	1.14	*	24.01	1.09	7.26	1.06	Dimercaprol	40.00	0.97					
Lasalocid sodium	22.84	1.09						Epiestriol	40.00	0.93					
Mundulone	22.94	1.06						Ethinyl estradiol	40.00	1.07					
BML-277	23.08	1.16	*	27.92	1.10	6.89	1.08	Gossypol-acetic acid complex	40.00	1.06					
Gossypol	24.29	1.14						H 89 2HCl	40.00	1.07					
L-162,313	24.74	1.15						Ivermectin	40.00	1.05					
Benzethonium chloride	25.24	0.92						Lomeguatrib	40.00	0.99					
Miconazole nitrate	26.29	1.08	*	38.22	1.11	18.97	1.06	Lopinavir	40.00	0.98					
Sorafenib	27.39	0.93	*	33.20	1.01	18.88	1.16	Milciclib (PHA-848125)	40.00	0.61					
Nelfinavir Mesylate	27.71	1.07						Miltefosine	40.00	0.99					
SKI II	27.97	0.84	*	40.00	0.96	12.91	1.05	Noradrenaline bitartrate H2O	40.00	1.02					
Elvitegravir	29.92	1.09						Nordihydroguaiaretic acid	40.00	1.09					
Indacaterol	30.08	1.19						Pazopanib HCl (GW786034 HCl)	40.00	0.43					
Sorafenib tosylate	30.85	0.82						Pelitinib (EKB-569)	40.00	1.00					
CP-471474	31.23	1.16	*	40.00	1.08	4.25	1.04	PF-562271	40.00	0.70					
Scriptaid	31.25	1.17	*	40.00	0.96	23.81	1.01	R(-)-Propylnorapomorphine HCl	40.00	1.06					
Oxiconazole nitrate	31.84	1.16						Rapamycin (Sirolimus)	40.00	1.05					
Sorafenib (Nexavar)	31.89	0.94						TNP	40.00	0.99					
Simvastatin	32.21	1.18						Tofacitinib (CP-690550) citrate	40.00	0.72					
Alexidine hydrochloride	32.49	1.07						Voxelotor	40.00	1.02					
Miconazole	32.54	1.12						WAY-600	40.00	0.93					

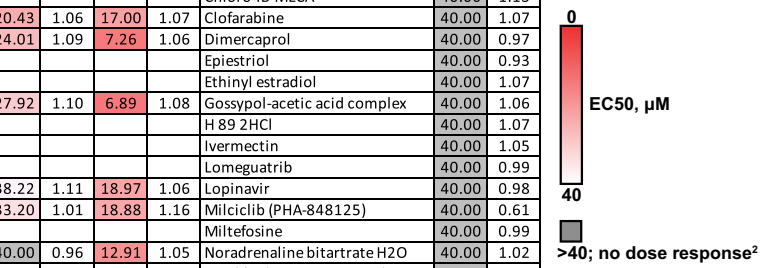

***Compounds repurchased from alternative vendor**
[1]N = normalized number of cells measured at indicated EC50 concentration compared to negative control
[2]no dose response below maximum concentration tested; value reported is single effective dose

B

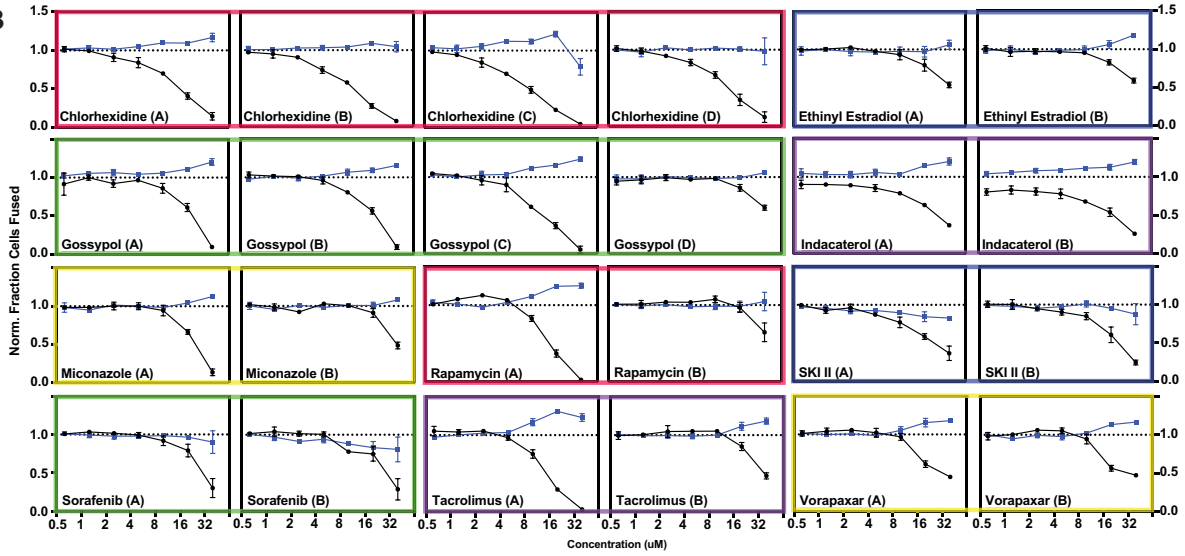

Figure 4—figure supplement 1. A drug repurposing screen implicates membrane lipid composition in cell-cell fusion. (**A**) Summary of 7-point dose-response for top-80 inhibitors in indicated heterokaryon assay (ACE2-U2OS vs. VeroE6). Asterisks reference compounds tested and validated by re-

Figure 4—figure supplement 1 continued on next page

Figure 4—figure supplement 1 continued

purchase from independent manufacturers. Heat-map indicates relative compound potency (bright red = higher). (**B**) Dose-response relationships for compounds (grouped by colored box) present in multiple small molecule libraries, each of whose replicates were identified as top-80 inhibitory hits. Mean and SEM: n = 3 biological replicates (16 images per).

A

Category	Parameter	Description	Non-hits (Means)	Hits (Means)	P-Value
Medicinal Chemistry	MW	Molecular Weight	343.85	490.37	2.20E-16
	HBA	Number of Hydrogen Bond Acceptors	4.29	5.3	0.001055
	HBD	Number of Hydrogen Bond Donors	1.86	2.93	8.29E-11
	LogP	n-Octanol/Water Partition Coefficient	1.94	4.13	2.20E-16
	RotB	Number of Rotatable Bonds	4.72	6.88	2.82E-10
	tPSA	Topological Polar Surface Area	84.7	103.24	0.00017
	LogD	n-Octanol/Water Distribution Coefficient	0.9	3.55	2.20E-16
Structural	N	Number of Nitrogen Atoms	2.12	3.1	0.0001347
	O	Number of Oxygen Atoms	3.66	4.25	0.778
	Rings	Number of Rings	2.78	3.63	2.99E-10
	ArRings	Number of Aromatic Rings	1.57	2.33	5.25E-10
	HetRings	Number of Heteroatom-containing Rings	1.21	1.61	0.0004862
	RingSys	Number of Ring Systems	1.81	2.54	9.60E-14
	SysRR	Ring Complexity	1.76	1.6	0.9188
Molecular Complexity & Recognition	Fsp^3	Fraction of sp^3 Hybridized Carbons	0.43	0.39	0.2219
	nStereo	Number of Stereocenters	2.18	3.28	0.1294
	ASA	Accessible Surface Area	526.49	701.16	2.20E-16
	relPSA	Relative Polar Surface Area	0.188	0.145	0.001241
	TC	Total Charge	0.036	0.392	0.0002149
	VWSA	van der Waals Surface Area	492.24	710.77	2.20E-16

B

Category	Parameter	Hits (Means)	GPCR Inhibitors (Means)	P-Value
Medicinal Chemistry	MW	490.37	432	9.68E-13
	HBA	5.3	4.2	3.75E-10
	HBD	2.93	3.16	0.000178
	LogP	4.13	1.78	5.05E-14
	RotB	6.88	8.13	0.0393
	tPSA	103.24	98.91	8.33E-11
	LogD	3.55	0.49	2.20E-16
Structural	N	3.1	3.41	0.2164
	O	4.25	3.51	0.001873
	Rings	3.63	3.16	0.0001853
	ArRings	2.33	1.89	4.80E-05
	HetRings	1.61	1.34	0.05283
	RingSys	2.54	2.18	0.0001503
	SysRR	1.6	1.67	0.5025
Molecular Complexity & Recognition	Fsp^3	0.39	0.46	0.000203
	nStereo	3.28	2.5	0.9194
	ASA	701.16	643.7	6.59E-09
	relPSA	0.145	0.13	5.41E-05
	TC	0.392	0.71	2.00E-11
	VWSA	710.77	653.47	8.94E-07

C

Scaffold	Scaffold count in hit library/Scaffold count in starting library	P-Value
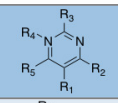	20/346	0.0114
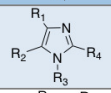	12/149	0.00132
	7/125	
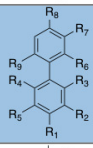	7/57	0.00046
	6/103	0.17702
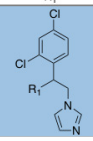	6/15	<0.00001
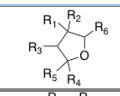	6/137	0.12602
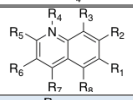	6/151	0.67448
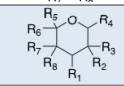	6/76	0.03572
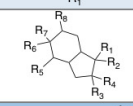	5/65	0.06228
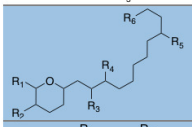	6/16	<0.00001
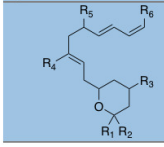	2/6	0.0005

Figure 4—figure supplement 2. A drug repurposing screen implicates membrane lipid composition in cell-cell fusion. (**A**) Analysis and comparison of 20 physicochemical properties for non-hit and hit libraries. P-values assessed with a Mann-Whitney U test. Dark and light blue represent p-values<0.001

Figure 4—figure supplement 2 continued on next page

Figure 4—figure supplement 2 continued

and<0.05, respectively. White indicates no significant differences. (**B**) Similar to (**A**), but inhibitory hits vs. a control GPCR inhibitor library obtained from literature. (**C**) List of top-10 most frequent scaffolds and substructures in the hit library as analyzed by Scaffold Hopper and RDKit Substructure Search, respectively. Enrichment significance relative to the starting library was assessed with two-tailed Z-scores used to calculate p-values. Dark and light blue represent p-values<0.001 and<0.05, respectively. White indicates no significant differences.

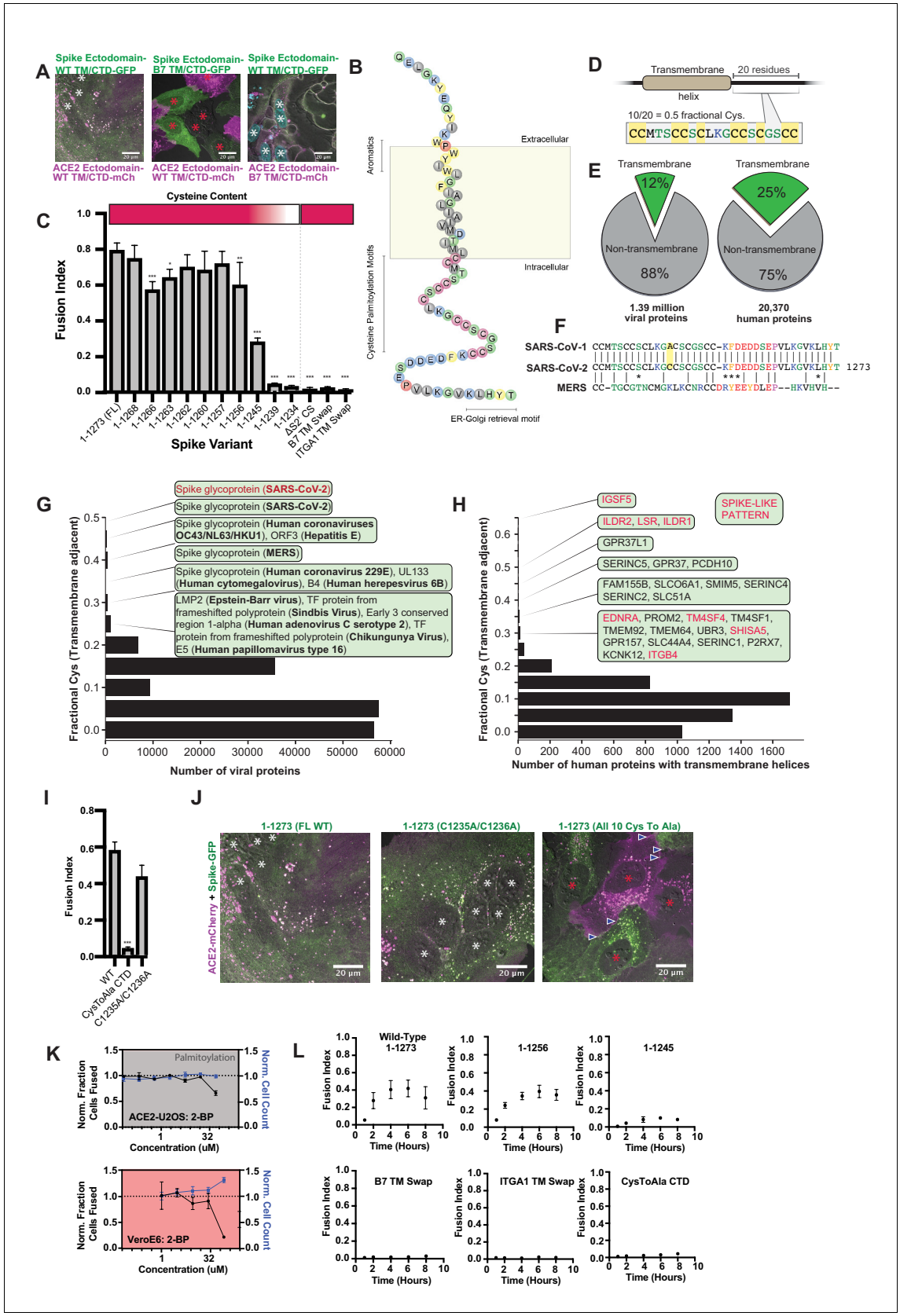

Figure 5. Highly unusual membrane-proximal regions of spike are needed for fusion. (**A**) Representative images of co-cultured (24 hr) U2OS cell lines, stably expressing indicated fluorescently tagged ACE2 or spike. 'B7 TM' indicates swap of endogenous transmembrane (TM) and cytoplasmic domain

Figure 5 continued on next page

Figure 5 continued

(CTD) of spike or ACE2 with that of the monomeric, single-pass, B7 transmembrane protein, along with its membrane-proximal extracellular region (30-amino acid spacer). White asterisks indicate nuclei in syncytia; red, in isolation. Note lack of arrowheads (synapses) in middle condition. See ***Supplementary file 4*** for residue composition of such 'chimeric' proteins. (**B**) Graphical representation of SARS-CoV-2 spike's TM alpha-helix and membrane-proximal regions, with residues colored by chemical properties (yellow, aromatic; cysteine, magenta; hydrophobic, gray; non-charged hydrophilic, green; charged hydrophilic; blue; proline, red). Of note: aromatic-rich region at ectodomain-TM interface, cysteine-rich cytoplasmic domain (CTD). (**C**) ACE2-U2OS heterokaryon assay but with co-cultured HNRNPA1-EYFP cells expressing spike variants (indicated). Relative CTD cysteine content for variants is depicted with heat map (top; dark red = more cysteines, white = none). Mean and SEM: n = 4 biological replicates (16 images per). See ***Figure 5—figure supplement 1B*** for all tested spike variants in both ACE2-U2OS and VeroE6 heterokaryon assays; ***Figure 5—figure supplement 1C***, for representative images of ACE2-mCherry U2OS cells co-cultured with GFP-tagged spike variants. p-values of <0.01, <0.001, and <0.0001 are represented by *, **, and ***, respectively. (**D**) Cartoon representation of SARS-CoV-2 spike with highest cysteine content in a 20-amino acid sliding window, which guided bioinformatic analyses shown in (**E–H**). (**E**) Schematic of bioinformatic analysis performed, whereby 20-residue windows around the N- and C-terminal sides of transmembrane helices were scanned for local cysteine density. Pie charts: summary of total set of viral proteins retrieved and analyzed for the human virus proteome (left) and human proteome (right); green slice references proportion of proteins with one or more predicted transmembrane helixes. (**F**) Conservation of cysteine-rich CTD between spike proteins of highly pathogenic human coronaviruses. The only difference between the CTD of SARS-CoV-1 and SARS-CoV-2 is acquisition of an additional cysteine in the latter. MERS is substantially different, yet retains enrichment of cysteines. (**G**) Histogram of fractional cysteine scores for viral proteins, with high-fraction hits explicitly annotated. SARS-CoV-2 spike protein has the highest local cysteine density of any viral protein, closely followed by spike proteins from other coronaviruses. (**H**) Similar to (**G**), but for human proteins with one or more predicted transmembrane helix. Red: 'spike-like' transmembrane proteins with high cytoplasmic cysteine content and aromatic residues at ectodomain-membrane interface. (**I**) Similar to (**C**), but using spike variants with cysteines mutated to alanine (2 of 10 vs. 10 of 10). (**J**) Representative images for 24 hr co-culture of ACE2-mCherry (magenta) U2OS cells with those expressing GFP-tagged spike variant (green). White asterisks indicate nuclei in syncytia; red, those in isolation; arrowhead, synapses (select examples noted). (**K**) Dose-response relationship for 2-bromopalmitate (2-BP, inhibitor of cysteine palmitoylation), in both ACE2-U2OS (top) and VeroE6 (bottom) heterokaryon assays. Blue indicates number of nuclei (proxy for toxicity); black, percent cells fused; both normalized to DMSO control. Mean and SEM: n = 4 biological replicates (16 images per). (**L**) Similar to (**C**), but assesses kinetics of fusion by varying co-culture time prior to fixation. See ***Figure 5—figure supplement 1A*** for other tested spike variants. See also ***Figure 5—figure supplement 1***; ***Supplementary files 2–4***.

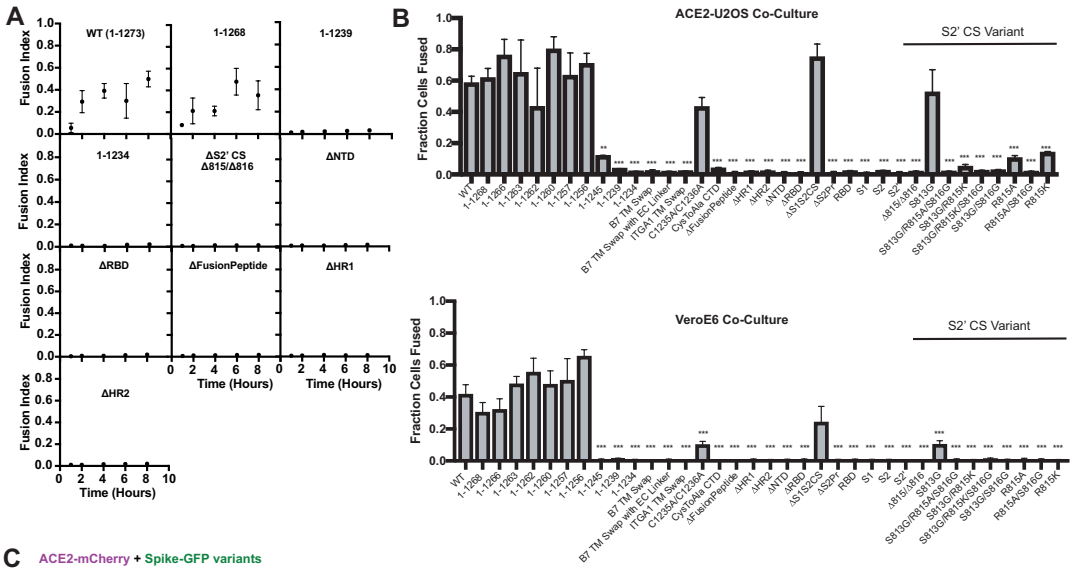

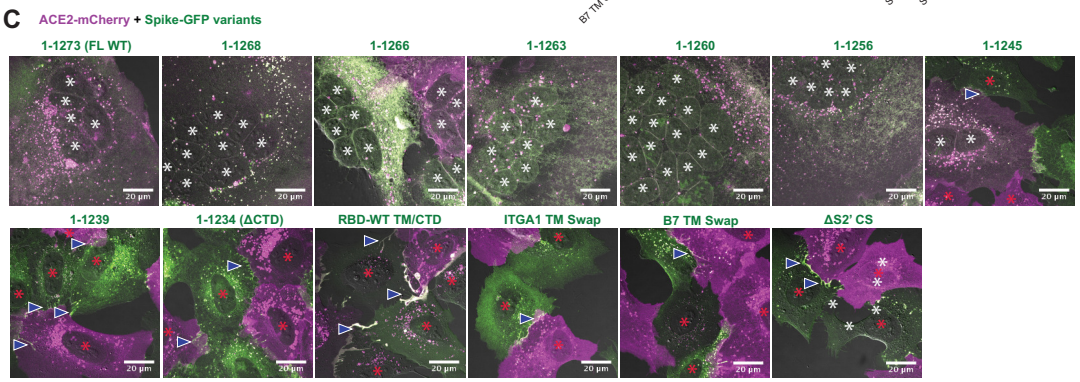

D

GO Molecular Function	#, Hu Prot (n=20851)	#, Cys-Rich (n=65)	Expected #, n=65	Enrich	P-Value	FDR
Prosaposin receptor	2	2	0.01	> 100	5.68E-05	3.86E-02
Endothelin receptor	2	2	0.01	> 100	5.68E-05	3.38E-02
Cargo receptor	76	4	0.24	16.88	1.13E-04	5.35E-02
Transmembrane signaling receptor	1319	18	4.11	4.38	7.91E-08	3.76E-04
Ion transmembrane transporter	890	12	2.77	4.33	1.88E-05	2.24E-02
Molecular transducer	1509	19	4.7	4.04	1.10E-07	2.61E-04
GO Cellular Component	**#, Hu Prot (n=20851)**	**#, Cys-Rich (n=65)**	**Expected #, n=65**	**Enrich**	**P-Value**	**FDR**
Prominosome	2	2	0.01	> 100	5.68E-05	7.11E-03
Tricellular tight junction	4	2	0.01	> 100	1.42E-04	1.57E-02
Ciliary membrane	77	4	0.24	16.66	1.18E-04	1.39E-02
Apical part of cell	439	7	1.37	5.12	4.58E-04	4.37E-02
Integral component of plasma membrane	1655	23	5.16	4.46	4.55E-10	1.52E-07
GO Biological Function	**#, Hu Prot (n=20851)**	**#, Cys-Rich (n=65)**	**Expected #, n=65**	**Enrich**	**P-Value**	**FDR**
(+)-reg. of serine C-palmitoyltransferase	3	3	0.01	> 100	5.69E-07	9.05E-03
(+)-reg. CDP-DAG-ser O-phosphatidyltransferase	3	3	0.01	> 100	5.69E-07	4.53E-03
Regulation of serine C-palmitoyltransferase	4	3	0.01	> 100	9.94E-07	3.95E-03

GO Molecular Function	#, Hu Prot (n=20851)	#, Spike-Like (n=15)	Expected #, n=15	Enrich	P-Value	FDR
Endothelin receptor	2	2	0	> 100	2.89E-06	1.38E-02
GO Cellular Component	**#, Hu Prot (n=20851)**	**#, Spike-Like (n=15)**	**Expected #, n=15**	**Enrich**	**P-Value**	**FDR**
Tricellular tight junction	4	2	0	> 100	7.22E-06	4.83E-03
Tight junction	128	3	0.09	32.58	1.04E-04	4.18E-02
GO Biological Function	**#, Hu Prot (n=20851)**	**#, Spike-Like (n=15)**	**Expected #, n=15**	**Enrich**	**P-Value**	**FDR**
None found	N/A	N/A	N/A	N/A	N/A	N/A

Figure 5—figure supplement 1. Highly unusual membrane-proximal regions of spike are needed for fusion. (**A**) ACE2-U2OS heterokaryon assay, but assesses kinetics of fusion by varying length of co-culture with spike variant (indicated)-expressing HNRNPA1-EYFP cells. Mean and SEM: n = 4

Figure 5—figure supplement 1 continued on next page

Figure 5—figure supplement 1 continued

biological replicates (16 images per). (**B**) Similar to (**A**) but for all studied spike variants at a single time-point (5 hr) and examined in both ACE2-U2OS (top) and VeroE6 (bottom) heterokaryon assays. Mean and SEM: n = 4 biological replicates (16 images per). p-values of <0.01, <0.001, and <0.0001 are represented by *, **, and ***, respectively. (**C**) Representative images of ACE2-mCherry (magenta) cells co-cultured for 24 hr with U2OS cells expressing GFP-tagged spike variant (green, labeled). White asterisks indicate nuclei in syncytia; red, in isolation; arrowhead, synapses between cells (select examples noted). (**D**) Top: Gene ontology (PantherDB) for cysteine-rich human transmembrane (TM) proteins, assessing significance of enrichment relative to the entire human proteome. Bottom: similar but for 'spike-like' human proteins (aromatics at TM interface, high cysteine content in cytoplasm CTD).

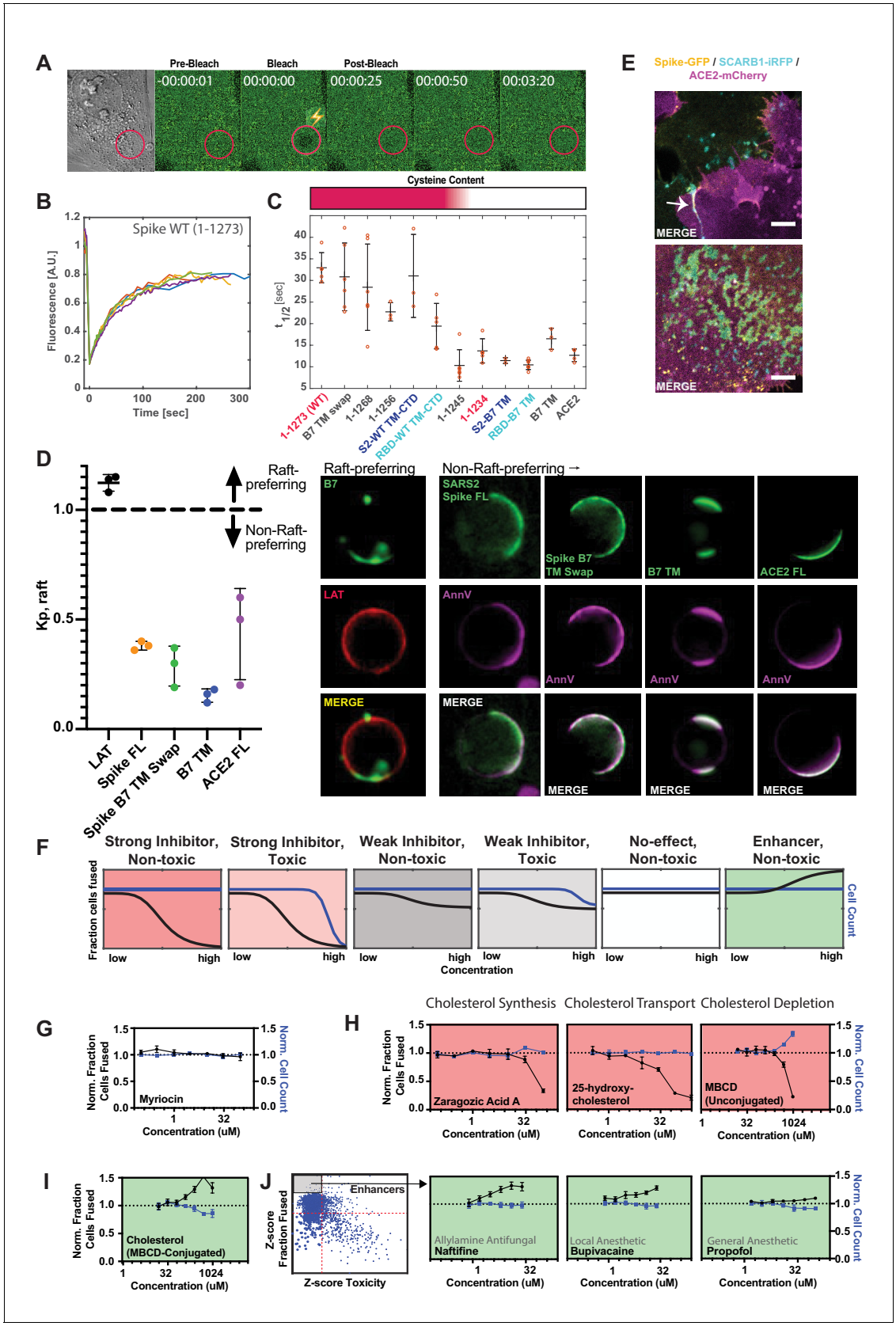

Figure 6. Spike requires membrane cholesterol for fusion but via a raft-independent mechanism. (**A**) Representative trial for fluorescence recovery after photobleaching (FRAP) of spike FL-GFP (green) on U2OS cell plasma membrane. Time since bleach (lightning bolt) of region of interest (red circle) is

Figure 6 continued on next page

Figure 6 continued

indicated. (**B**) Quantification of (**A**) and related trials, with each colored line specifying a separate FRAP experiment (n = 6 total). (**C**) Calculated half maximal fluorescence recovery ($t_{1/2}$) for indicated GFP-tagged spike variants. Each hollow red dot indicates the $t_{1/2}$ for a single FRAP trial. Mean and SEM: n = 4–6 technical replicates (one per cell). Heat map (top): relative cysteine content of tested spike variant (dark red = high cysteine content, white = none). (**D**) Ex vivo phase separation assay for relative partitioning (K_p) into lipid raft ordered phase (L_o) of giant plasma membrane vesicles (GPMVs). Left: quantification of GFP-tagged protein K_p with DHPE serving as lipid raft/L_o marker; AnnV, non-raft/L_d protein marker; LAT, raft/L_o protein marker. Mean and SEM: n = 3 biological replicates (colored dot;>10 GPMV technical replicates per). Right: representative images. (**E**) U2OS cells expressing spike-GFP (yellow) and SCARB1-iRFP (cyan) were co-cultured with ACE2-mCherry (magenta) cells and cell-cell fusion events were captured with live cell microscopy. Representative images show co-localization between spike and SCARB1 at synapses that precede fusion (top, arrow); and in extracellular deposits (bottom). Scale-bar, 5 μm. See ***Figure 6—figure supplement 1A,B*** for individual fluorescence channels. (**F**) Graphical schematic for ACE2-U2OS assay dose-response and interpretation. Fraction of cells fused (black curve) relative to cell count (blue curve), both normalized by the plate negative control, indicates compound effectiveness (pink, strong inhibitor; gray, weak inhibitor; white, no-effect; green, enhancer). (**G**) Lack of dose-dependent inhibition of fusion by sphingolipid-depleting, and raft-disrupting drug, myriocin, in ACE2-U2OS heterokaryon assay. Mean and SEM: n = 4 biological replicates (16 images per). (**H**) Similar to (**G**), but measuring effect of cholesterol-lowering drugs in ACE2-U2OS heterokaryon assay. Mean and SEM: n = 4 biological replicates (16 images per). (**I**) Similar to (**G**), but with MBCD-conjugated cholesterol, which increases plasma membrane cholesterol content. See ***Figure 6—figure supplement 1E*** for controls (i.e. other MBCD-conjugated lipids). (**J**) Similar to (**G**), but testing potential fusion-enhancing compounds (see ***Figure 4B***, gray inset), which include allylamine antifungals (e.g. naftifine) and anesthetics (e.g. bupivacaine, propofol). See ***Figure 6—figure supplement 1F*** for similar effects by other small molecules belonging to these compound classes. See also ***Figure 6—figure supplement 1***; ***Supplementary file 4***.

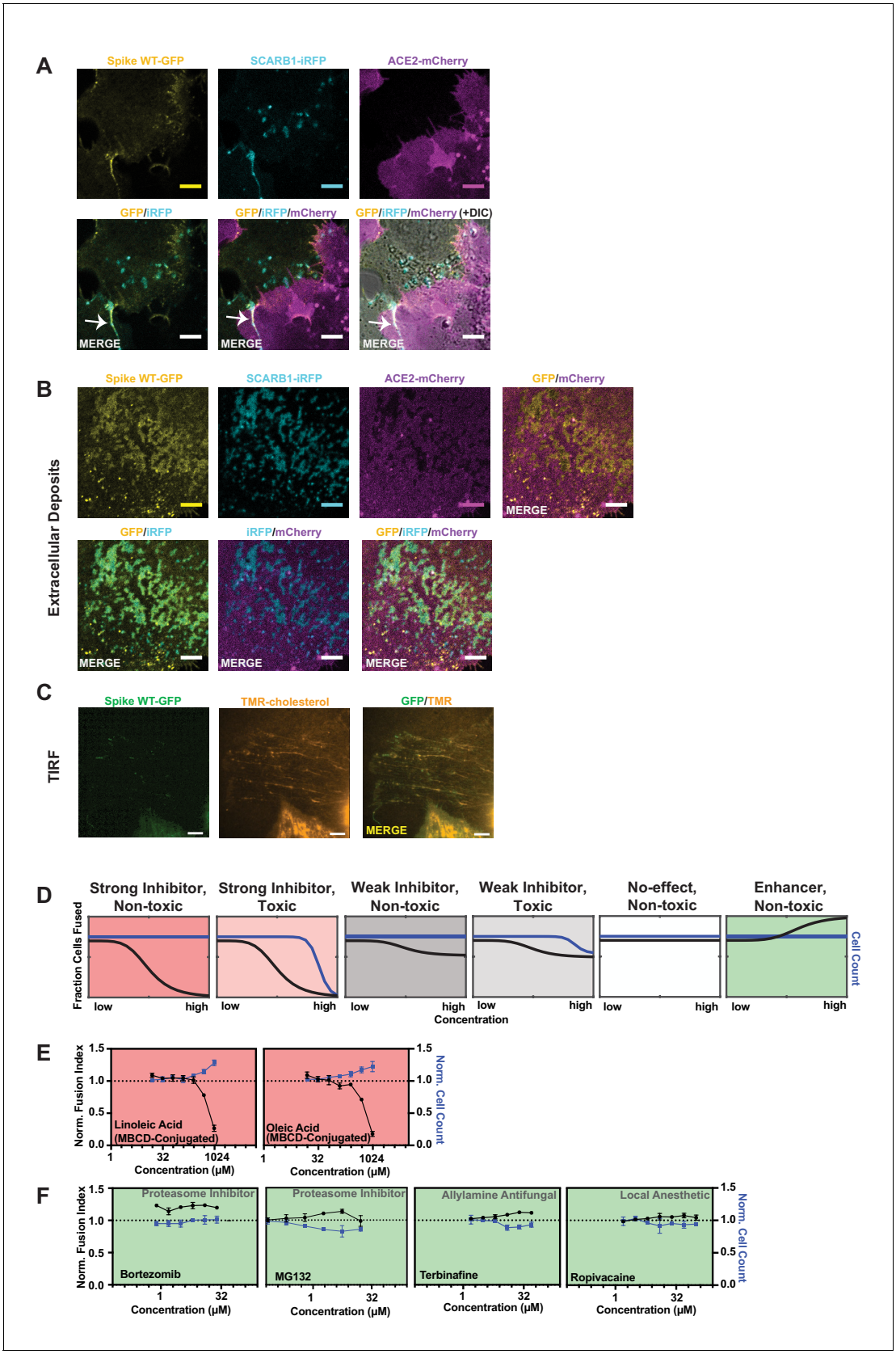

Figure 6—figure supplement 1. Spike requires membrane cholesterol for fusion via a raft-independent mechanism. (**A**) Individual fluorescence channels for merge image shown in ***Figure 6E*** (top). Arrow indicates co-localization between cholesterol-binding protein SCARB1-iRFP (cyan) and

Figure 6—figure supplement 1 continued on next page

Figure 6—figure supplement 1 continued

spike-GFP (yellow) at transcellular synapses. (**B**) Individual fluorescence channels for merge image shown in ***Figure 6E*** (bottom). (**C**) Representative images of extracellular membrane deposits that contain both cholesterol (CholEsteryl-BODIPY stain, orange) and spike-GFP (green). (**D**) Graphical schematic for ACE2-U2OS assay dose-response and interpretation. Fraction of cells fused (black curve) relative to cell count (blue curve), both normalized by the plate negative control, indicates compound effectiveness (pink, strong inhibitor; gray, weak inhibitor; white, no-effect; green, enhancer). (**E**) Dose-response analysis of control MBCD-conjugated lipids in ACE2-U2OS heterokaryon assay. Black line indicates fraction of cells fused; blue, cell count (toxicity measure); both of which are normalized to DMSO negative control. Mean and SEM: n = 4 biological replicates (16 images per). (**F**) Similar to (**E**), but with compounds predicted by drug repurposing screen to enhance fusion. Drug class indicated.

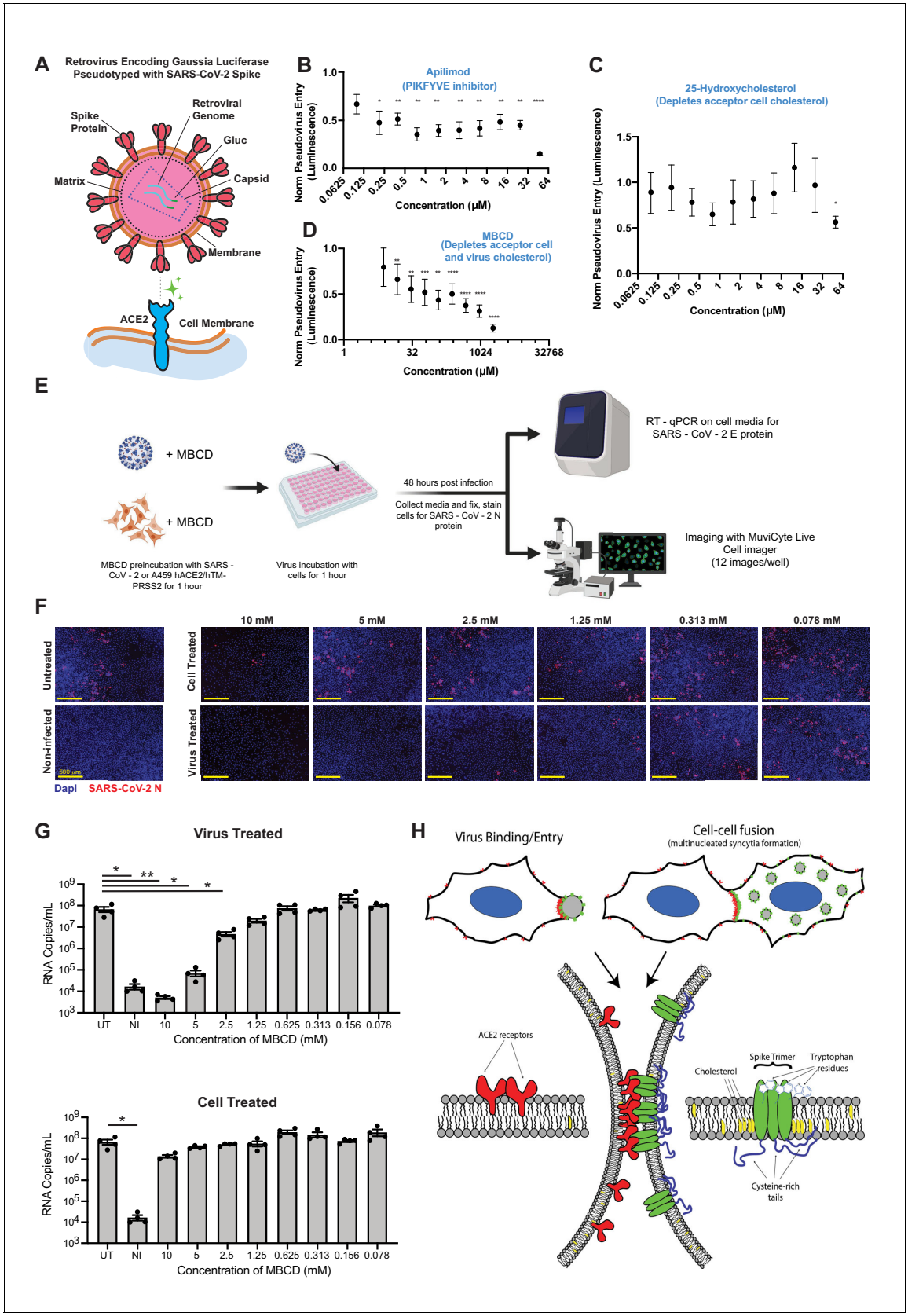

Figure 7. SARS-CoV-2 infection depends on membrane cholesterol of the virus but not the host cell. (**A**) Schematic representation of pseudotyped virus entry assay in ACE2/TMPRSS2-expressing A549 acceptor cells, which are primarily infected via direct fusion pathway. Pseudovirus encodes *Gaussia*

Figure 7 continued on next page

Figure 7 continued

luciferase gene, which allows luminescence-based measure of relative entry as a function of compound concentration. (**B**) Dose-dependent inhibition of pseudovirus entry (luminescence, arbitrary units) for a positive control compound (apilimod, PIKFYVE inhibitor), relative to control (1 = no effect; 0 = complete block). Mean and SEM indicated for six replicates. P-values of <0.05, <0.01, <0.001, and <0.0001 are represented by *, **, *** and ****, respectively. (**C**) Similar to (**B**), but for cholesterol-transport disrupting drug, 25-hydroxycholesterol. (**D**) Similar to (**B**), but for plasma membrane cholesterol-stripping compound, MBCD. (**E**) Schematic of SARS-CoV-2 infection assays in ACE2/TMPRSS2 A549 acceptor cells. Relative infection is determined by RT-qPCR or immunohistochemistry of the SARS-CoV-2 nucleocapsid protein (N). (**F**) Representative immunofluorescence (nucleocapsid protein, red; nuclei/DAPI, blue) of A549 cells, 48 hr post-infection by SARS-CoV-2. Top: cells pre-treated with indicated dose of MBCD, followed by wash; bottom: pre-treatment of virus. (**G**) Similar to (**F**), but using RT-qPCR to quantify viral titer (RNA copies per mL cell media) following MBCD-treatment of virus (top) or cells (bottom). Identical controls plotted on both graphs for visualization purposes: UT = untreated cells, NI = non infected cells. Mean and SEM indicated for n = 4 independent biological replicates (black dots). p-values of <0.05 and<0.01 are represented by * and **, respectively. (**H**) Graphical model of the biomolecular interactions required for SARS-CoV-2 spike-mediated membrane fusion. Bottom: palmitoylated cysteines (blue) act as multivalent membrane contacts, anchoring trimeric spike peplomers (green) to the phospholipid bilayer (black) and potentially allowing transient higher order assemblies of trimers. Aromatic residues (e.g. tryptophans) at the spike ectodomain-membrane interface associate with accessible cholesterol (yellow) to promote synapse-like clusters with ACE2 receptors (red) on apposing membranes. Without these collective interactions, spike's fusion machinery (e.g. fusion peptide and heptad repeats) is unable to surmount the energetically costly barrier to lipid bilayer mixing, both in virus-cell (top, left) and cell-cell fusion (top, right).